Zero-order bows in radially inhomogeneous spheres: direct and inverse problems

John A. Adam

Department of Mathematics and Statistics, Old Dominion University, Norfolk, Virginia 23508, USA (jadam@odu.edu)

Received 7 April 2011; revised 25 July 2011; accepted 26 July 2011; posted 29 July 2011 (Doc. ID 145522); published 6 September 2011

Zero-order ray paths are examined in radially inhomogeneous spheres with differentiable refractive index profiles. It is demonstrated that zero-order and sometimes twin zero-order bows can exist when the gradient of refractive index is sufficiently negative. Abel inversion is used to "recover" the refractive index profiles; it is therefore possible in principle to specify the nature and type of bows and determine the refractive index profile that induces them. This may be of interest in the field of rainbow refractometry and optical fiber studies. This ray-theoretic analysis has direct similarities with the phenomenon of "orbiting" and other phenomena in scattering theory and also in seismological, surface gravity wave, and gravitational "lensing" studies. For completeness these topics are briefly discussed in the appendixes; they may also be of pedagogic interest.

OCIS codes: 000.3860, 000.3870, 080.2720, 080.5692, 110.3200, 260.2710.

1. Introduction

It is well known that sun-illuminated homogeneous raindrops cannot produce zero-order (or direct transmission) rainbows. In other words, there is no extremum in the angle of deviation for geometrical light rays transmitted directly through the sphere. It is also known that such bows *can* exist when the drops have an elliptical cross section or the source of illumination is sufficiently close to the drops [1].

A ray-theoretic account of the passage of light through a radially inhomogeneous transparent sphere established [2] the existence of *multiple* primary bows for some refractive index profiles. One of the aims of the present paper is to show that such bows can also occur in direct transmission. The existence of such additional bows is a consequence of a sufficiently attractive potential in the interior of the drop, i.e., the refractive index gradient should be sufficiently negative there. Profiles for which this gradient is monotonically increasing are not expected in general to result in this phenomenon, but nonmonotone profiles $n(r)$ definitely can do so. Sufficiently oscillatory profiles can lead to apparently singular behavior in the deviation angle (within the geometrical optics approximation) as well as multiple bows.

Given that bows can exist, even for direct transmission, it is of interest to examine the related inverse problem, namely to determine the refractive index profiles that give rise to these bows. This involves inverting an Abel integral equation [3–5], a topic that has received attention in a wide range of fields, especially in recent years. Abel inversion techniques have been used in fields such as x-ray radiography [6–8], galactic astronomy [9,10], optical fiber evaluation (extensively so, see [11–25]), satellite photometry using radio occultation techniques [26–33], microscopy, plasma electron diagnostics [34–37], and seismology [38–40]. In particular, radio occultation experiments using radio links between the Earth spacecraft that pass behind planets as seen from Earth have provided valuable information about planetary atmospheres. Mariner V radio occultation measurements have provided profiles for refractivity, molecular number density, pressure, and temperature distributions for the Venusian atmosphere, amongst other properties [27]. Indeed, as pointed out by Eshleman [28], molecular atmospheres, ionospheres. magnetospheres, particulate

0003-6935/11/280F50-10$15.00/0

atmospheres, and some general relativistic "fields" can all affect radio signal characteristics. The classic example of the latter is the deflection of light by the Sun, predicted by Einstein in 1915. Similar studies in seismology use the "bend angle" to infer the properties of the underlying layers in the Earth [38]. The topics of gravitational, seismic, and surface gravity wave lensing are briefly addressed in the appendixes to elucidate the ubiquity of these techniques within the broader field of scattering theory.

2. Ray Path Integral

In what follows, i refers to the angle of incidence for the incoming ray, r is the radial distance within the *unit* sphere, and $D(i)$ is the deviation undergone by the ray. Below, the subscripts 0 and 1 will be used to distinguish the deviations of the exiting ray for direct transmission and the primary bow, respectively. In a spherically symmetric medium with refractive index $n(r)$, each ray path satisfies the following equation:

$$rn(r)\sin\phi = \text{constant}, \tag{1}$$

where ϕ is the angle between the radius vector $\bar{r}$ and the tangent to the ray at that point. This expression may be thought of as the optical analogue of the conservation of angular momentum for a particle moving under the action of a central force. The result, known as Bouguer's formula (for Pierre Bouguer, 1698–1758), implies that all the ray paths $r(\theta)$ are curves lying in planes through the origin (θ is the polar angle). Elementary differential geometry establishes that

$$\sin\phi = \frac{r(\theta)}{\sqrt{r^2(\theta)+(dr/d\theta)^2}}. \tag{2}$$

From this the angular deviation of a ray $\Theta(i)$ within the sphere can be determined and subsequently the total angle of deviation $D(i)$ through which an incoming ray at angle of incidence i is rotated. This gives the same formula for $\Theta(i)$ (see Fig. 1) as the method using Bouguer's formula; indeed, the two are equivalent. Thus,

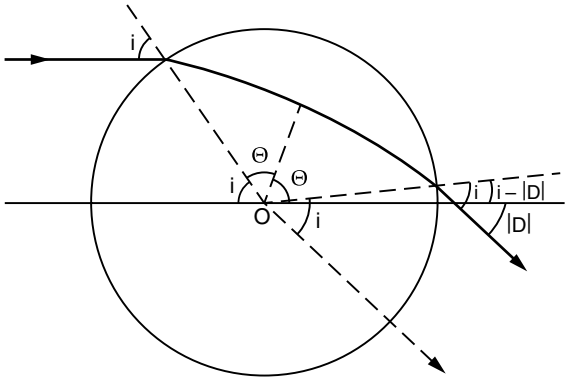

Fig. 1. Ray path for direct transmission through a radially inhomogeneous sphere for $n'(r) < 0$.

$$\Theta(i) = \sin i \int_{r_c(i)}^{1} \frac{dr}{r\sqrt{r^2n^2(r)-\sin^2 i}}. \tag{3}$$

The lower limit $r_c(i)$ is the point at which the integrand is singular and is therefore the solution of Eq. (4) in which (for a *unit* sphere), $\sin i$ is the *impact parameter*. $r_c(i)$ is the radial point of closest approach to the center of the sphere, sometimes called the *turning point*. The value of is determined implicitly from the following expression:

$$\eta(r_c(i)) \equiv r_c(i)n(r_c(i)) = \sin i. \tag{4}$$

The nature of $\eta(r) = rn(r)$ will be very significant in what follows; in particular, $r_c(i)$ will be unique if $\eta(r)$ is a monotonic function. As noted below, the integral in Eq. (3) can be evaluated analytically in certain special cases. Ray paths can also be determined by Fermat's principle; in terms of arc length s along the ray, the variation

$$\delta\int n(r)ds = 0,$$
$$\text{i.e.,}\ \delta\int n(r)\left[1+r^2\left(\frac{d\theta}{dr}\right)^2\right]^{1/2}dr = 0, \tag{5}$$

from which $\theta(r)$ [or $r(\theta)$] can be determined. Indeed, the Euler–Lagrange equation for the above variational principle is

$$\frac{d}{dr}\left\{n(r)\frac{r^2(d\theta/dr)}{[1+r^2(d\theta/dr)^2]^{1/2}}\right\} = 0, \tag{6}$$

and this yields Eq. (3) also.

A well-known result is that the curvature of the ray path is toward regions of higher refractive index n. This is a consequence of Snell's law of refraction generalized to continuously varying media. Thus, within the sphere, if $n'(r) < 0$, an incoming ray is concave toward the origin; if $n'(r) > 0$, it is convex toward the origin. From Fig. 1 it can be seen that, for direct transmission,

$$i + 2\Theta + (i - |D_0(i)|) = \pi \Rightarrow |D_0(i)| = 2i - \pi + 2\Theta. \tag{7}$$

It is readily noted that, for one internal reflection (corresponding to a primary bow),

$$|D_1(i)| = 2i - \pi + 4\Theta. \tag{8}$$

In what follows the absolute value notation will be dropped. The deviation formulas can be extended to higher-order bows in an obvious fashion.

Analytic expressions for $\Theta(i)$ are difficult to obtain except for a few specific $n(r)$ profiles; several examples are indicated below. For a constant refractive index, $\Theta(i)$ is a standard integral resulting in the inverse secant function and can be readily evaluated. Specifically,

$$D_0(i) = 2i - 2\tilde{r}(i), \tag{9a}$$

$$D_1(i) = 2i + \pi - 4\tilde{r}(i), \tag{9b}$$

where $\tilde{r}(i)$ is the angle of refraction inside the sphere. Of course, these results are readily determined from elementary geometry. As already noted, there can be no "zero-order rainbow" for the direct transmission of sunlight, only primary and secondary bows (ignoring theoretically possible but practically almost unobservable higher-order bows). In Fig. 2 the dashed curve D_h represents the deviation $D_1(i)$ through a sphere of *constant* refractive index $n = 4/3$. The other graphs represent the deviations corresponding to a zero bow and a primary bow for the particular (but arbitrary) choice of refractive index

$$n_1(r) = 1.3 - 0.2\cos\{[1.9(r - 0.85)]^2\}. \tag{10}$$

This profile is one that will be recovered by Abel inversion in Section 4. Note that both $D_0(i)$ and $D_1(i)$ exhibit fairly broad double extrema in this case. It is interesting to note that the relative maximum for D_1 is much less pronounced than that for D_0. The reverse is true for the profile

$$n_2(r) = 1.1\{1 - [0.55(1 - r)]^2\}^{-1} \tag{11}$$

as shown in Fig. 3. These are just examples from a wide range of $n(r)$ profiles inducing such $D_k(i)$ curves ($k = 0, 1$); indeed, for

$$n_3(r) = 1.33 + 0.23\cos\{[1.8(r - 0.1)]^2\}, \tag{12}$$

a triple *primary* bow was found (Fig. 4).

With regard to more general analytic profiles for which the deviation integral can be evaluated exactly, the (somewhat unphysical) power law profile $n(r) = n(R)(r/R)^m$, where m can be of either sign, was chosen for a sphere of radius R ([41]; see also [42]), and by a judicious change of variable this can be reduced to the standard result for a constant refractive index. Several ray paths for this highly "attractive" profile (for $m < 0$) are illustrated in Fig. 5 below. For the choice of a "shifted hyperbolic" profile of the form $n(r) = (ar + b)^{-1}$, the integral Eq. (3) can be evaluated in terms of elementary transcendental functions [2]. The complexity of these integrals increases rapidly with even relatively simple expressions for $n(r)$. For a linear profile, Eq. (3) can be evaluated in terms of incomplete elliptic integrals of the first and third kinds. In [43] a parabolic profile of the form $n(r) = a - br^2$ also yields a result also in terms of a purely imaginary elliptic integral of the third kind. Related numerical studies can be found in [44–47].

Whether the ray path integral is evaluated analytically or numerically, it contributes to the *direct problem* of geometrical optics, namely (for direct transmission) the total angular deviation $2\Theta(i)$ of the ray inside the sphere for a given profile $n(r)$. Coupled with the refraction at the (in general discontinuous) boundary entrance and exit points this naturally yields the total deviation of an incoming ray as a function of its angle of incidence. The corresponding *inverse problem* is to determine the profile $n(r)$ from knowledge of the quantity $\Theta(i)$. This is generally more difficult to accomplish, and from a strict mathematical point of view, inverse problems in

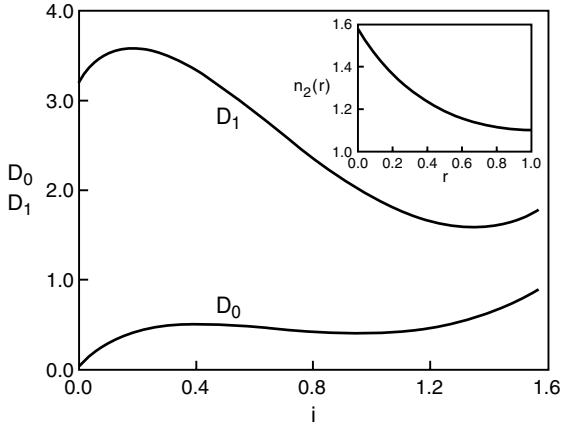

Fig. 3. Deviation functions (D_0 and D_1) for an inhomogeneous sphere for the profile (inset) $n_2(r)$.

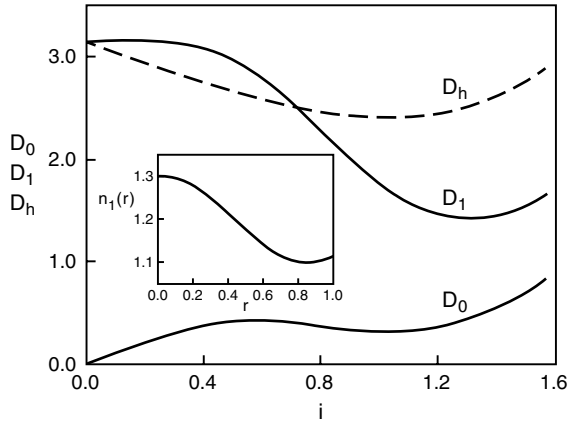

Fig. 2. Deviation functions for both a homogeneous (D_h) and inhomogeneous spheres (D_0 and D_1) for the profile (inset) $n_1(r)$.

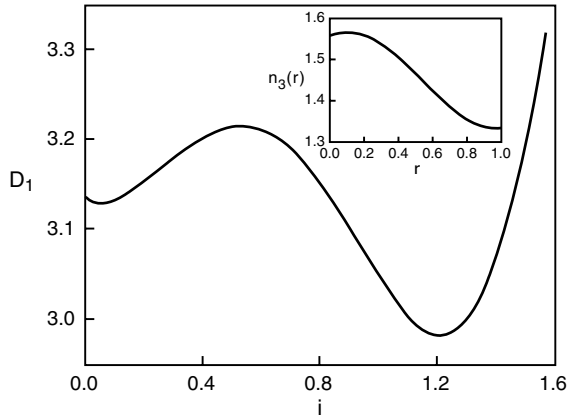

Fig. 4. Deviation function for a *primary* bow (D_1) from an inhomogeneous sphere with the profile (inset) $n_3(r)$.

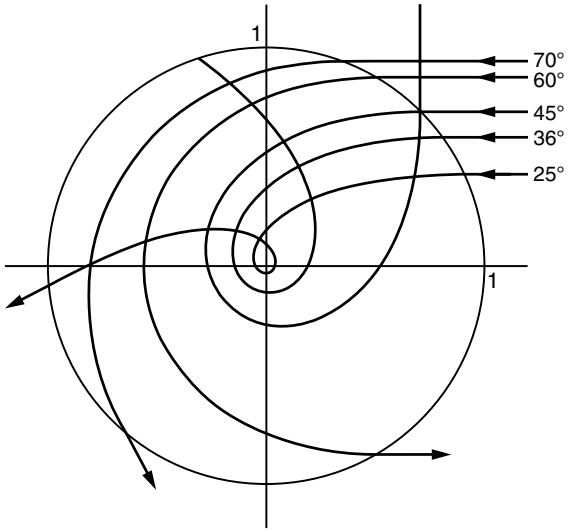

Fig. 5. Ray paths for a refractive index profile $n(r) = n(1)r^m$, $m = -0.75$ here (see [41]).

general are notorious for their lack of solution uniqueness. In practical terms it is not significant in this context, and we shall address the topic no further here.

3. Inverse Problem: Theory

To construct $n(r)$ as the solution to the inverse problem, we presume that $\Theta(i)$ is known, either analytically or numerically. We now define $2\Theta(i) = 2\Theta(\arcsin p) \equiv \Delta(p)$, where $p = \sin i$. Rewriting the radius of closest approach for a given i as η_i, we have

$$\Delta(p) = 2\int_{r_c(i)}^{1} \frac{p}{r}\frac{\mathrm{d}r}{(\eta^2 - p^2)^{1/2}} = 2\int_{p}^{\eta_0} \frac{p}{r}\frac{1}{(\eta^2 - p^2)^{1/2}}\frac{dr}{d\eta}\mathrm{d}\eta, \tag{13}$$

where η_0 is the value of η corresponding to an impact parameter of one; that is, $\eta_0 = n(1)$. Equation (13) is a form of Abel's integral equation, and in what follows "Abel inversion" is carried out to arrive at an expression that will ultimately lead to a reconstruction of $n(r)$. Multiplying Eq. (13) by $(p^2 - \eta_i^2)^{-1/2}$ and integrating with respect to p from η_i to η_0 results in the iterated integral

$$\int_{\eta_i}^{\eta_0} \frac{\Delta(p)}{(p^2 - \eta_i^2)^{1/2}}\mathrm{d}p = \int_{\eta_i}^{\eta_0} \mathrm{d}p \times \int_{p}^{\eta_0} \frac{2p}{r}\left\{\frac{1}{(p^2 - \eta_i^2)^{1/2}(\eta^2 - p^2)^{1/2}}\right\}\frac{dr}{d\eta}\mathrm{d}\eta. \tag{14}$$

Changing the order of integration on the right-hand side yields the integral

$$\int_{\eta_i}^{\eta_0} \mathrm{d}\eta \int_{\eta_i}^{\eta} \frac{2p}{r(p^2 - \eta_i^2)^{1/2}(\eta^2 - p^2)^{1/2}}\frac{dr}{d\eta}\mathrm{d}p. \tag{15}$$

Now the integral

$$\int_{\eta_i}^{\eta} \frac{p}{r(p^2 - \eta_i^2)^{1/2}(\eta^2 - p^2)^{1/2}}\mathrm{d}p = \left[\arcsin\left(\frac{p^2 - \eta_i^2}{\eta^2 - \eta_i^2}\right)\right]_{p=\eta_i}^{p=\eta} = \frac{\pi}{2}, \tag{16}$$

so that

$$I(\eta_i) \equiv \int_{\eta_i}^{\eta_0} \frac{\Delta(p)}{(p^2 - \eta_i^2)^{1/2}}\mathrm{d}p = \int_{\eta_i}^{\eta_0} \frac{\pi}{r}\frac{dr}{d\eta}\mathrm{d}\eta = \pi[\ln r]_{r_c(i)}^{1} = -\pi \ln r_i(i). \tag{17}$$

This will be the form used for the numerical inversion, but for analytic purposes the following additional representation is sometimes useful [26,48]. If $p = \eta_i \cosh\lambda$ is substituted in the left-hand side of this equation, on integrating by parts we have

$$I(\eta_i) = \left[\Delta(p)\operatorname{arccosh}\left(\frac{p}{\eta_i}\right)\right]_{\eta_i}^{\eta_0} - \int_{\eta_i}^{\eta_0} \operatorname{arccosh}\left(\frac{p}{\eta_i}\right)\frac{d\Delta}{dp}\mathrm{d}p. \tag{18}$$

Now $[\Delta(p)]_{\eta_0} = 0$ so the integrated term is zero. Therefore,

$$I(\eta_i) = -\int_{\eta_i}^{\eta_0} \operatorname{arccosh}\left(\frac{p}{\eta_i}\right)\frac{d\Delta}{dp}\mathrm{d}p = \int_{\Delta(\eta_i)}^{\Delta(\eta_i)} \operatorname{arccosh}\left(\frac{p}{\eta_i}\right)\mathrm{d}\Delta = -\pi \ln r_i(i). \tag{19}$$

Returning to Eq. (17), we invert it to obtain

$$r_i(\eta_i(i)) = \exp\left[-\frac{I(\eta_i)}{\pi}\right]. \tag{20}$$

This equation gives the radius of closest approach, $r_i(i)$, that is, a particular value of r for a given value of i, expressed as a function of η_i [a particular value of $rn(r)$]. Some points of closest approach for several ray paths are shown in Fig. 6 (using the notation of Fig. 11 in Appendix A).

Note that η_i and $r_i(i)$ are the corresponding values for the same ray path, related by the Bouger formula $\eta_i = \eta(r_i(i)) \equiv r_i(i)n(r_i(i))$. From these two equations, the refractive index $n(r)$ can be obtained from the ray bending angle $\Delta(p)$, which in turn can be measured experimentally (or defined theoretically); this will determine the corresponding profile $n(r)$. Since $\eta_i = n(r_i)r_i > r_i$, we can regard η_i as a different (and larger) value of r_i. Then we have

$$n(r(\eta_i)) = \frac{\eta_i}{r_i(\eta_i)} = \eta_i \exp[I(\eta_i)/\pi]. \tag{21a}$$

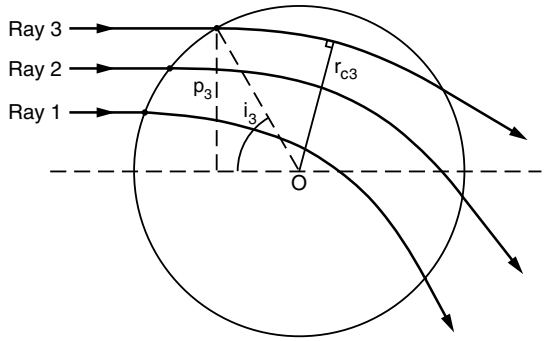

Fig. 6. Typical ray paths with corresponding points r_{ci} of closest approach to the center O (only details for ray 3 are shown for clarity).

Clearly, we may now write the refractive index profile generically as

$$n(r) = r\exp[I(r)/\pi]. \tag{21b}$$

An alternative formulation is to find $n(r(\eta_i))$ first and then use the Bouger formula to obtain the corresponding value $r(\eta_i)$ and that way to recover the profile $n(r)$ [27,28]. It follows from Eq. (21b) that the refractive index will have an extremum if $I'(r) = -\pi/r$ [assuming this occurs with the interval $(0,1)$]. This is indeed the situation for the nonlinear profiles discussed here. In all the cases examined above, in fact, $I(r)$ has the same qualitative features, being of the general form $I(r) = \beta r^{-\alpha} + \gamma$ for α, β, and γ all being positive constants. If this can be fitted to a given numerical form for I, then $n'(r) = 0$ when $r = (\alpha\beta/\pi)^{1/\alpha}$. This is unique of course; other profiles for which n has multiple extrema will give rise to different functional forms for the integral I. In the case of the profiles considered, the graphs of $I'(r)$ and $-\pi/r$ intersect once for nonlinear profiles and not at all in $(0,1)$ for the linear profiles (as should be the case).

In Figs. 7 and 8, the efficacy of the Abel inversion has been tested by simply evaluating the integral Eq. (3) for $\Theta(i)$ [and specific profiles $n(r)$], expressed as a function of p, and then substituting it back into the following integral in Eq. (17) above, namely

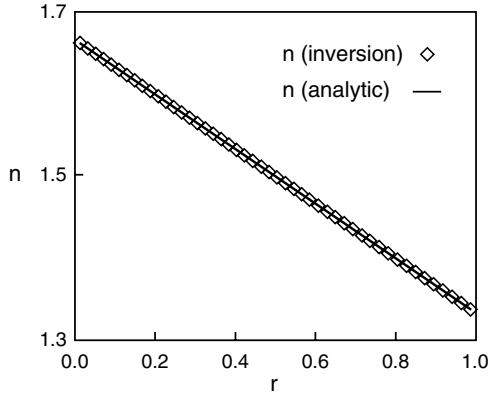

Fig. 7. Refractive index profile $n(r) = (5 - r)/3$ and its Abel inversion.

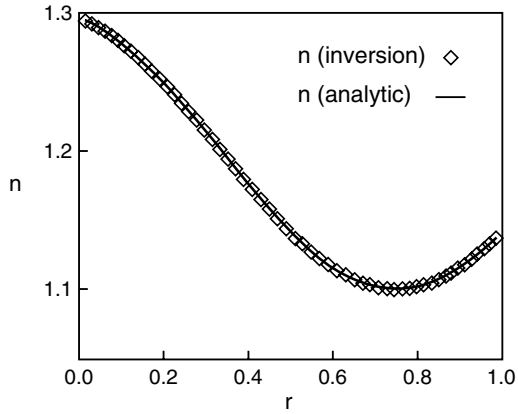

Fig. 8. Refractive index profile $n(r) = 1.3 - 0.2\cos\{[1.9(r - 0.85)]^2\}$ and its Abel inversion.

$$I(\eta_i) \equiv \int_{\eta_i}^{\eta_0} \frac{\Delta(p)}{(p^2 - \eta_i^2)^{1/2}}\,\mathrm{d}p. \tag{22}$$

Then Eq. (21a) is used to calculate the recovered refractive index profile. In Fig. 7 the profile $n(r) = (5 - \alpha r)/3$ for $\alpha = 1$ is compared with its reconstruction using the Abel inversion (21a) and (22).

It should be noted that no zero bow occurs in this case. Indeed, the behavior of $D_0(i)$ is very interesting as α is varied. Numerically, it appears that no bows [i.e., extrema of $D_0(i)$] occur for $\alpha < 1.885$ approximately; for α in the approximate range (1.885, 1.999) there exist double zero bows, and for $\alpha = 2$ there is a single bow ($\alpha > 2$ is unphysical for $r > 2\alpha^{-1}$). Thus, it appears in this case that the profile gradient $n'(r) = -\alpha/3$ should be sufficiently negative, an observation noted in [2] in connection with the existence of multiple primary bows. Figure 8 illustrates the corresponding reconstruction for the profile given by Eq. (10), namely

$$n(r) \equiv n_1(r) = 1.3 - 0.2\cos\{[1.9(r - 0.85)]^2\}.$$

4. Inverse Problem: Additional Comments

We can readily relate the "inversion of Δ" to the more valuable "inversion of D," the measured total deviation angle of the incident ray. From Eq. (7), in terms of p,

$$\Delta(p) = D_0(\arcsin p) - 2\arcsin p + \pi. \tag{23}$$

In Eq. (17) the quantity $\Delta(p)$ is characterized by a monotonically decreasing function, illustrated as $\Delta_{0l}(p)$ in Fig. 9, in this case for the linearly decreasing profile

$$n(r) = \frac{4 - r}{3}. \tag{24}$$

A similar result arises for any other linearly decreasing profile; it is not necessary that $n(1) = 1$

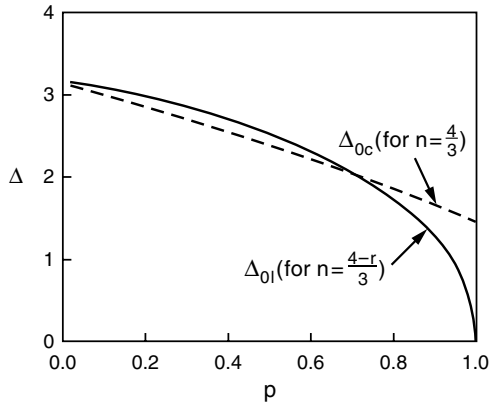

Fig. 9. Within-sphere angular deviation $\Delta(p)$ for the profile Eq. (24) (solid line) and a constant profile (dashed line).

as here. Also shown for comparison for a constant $n = 4/3$ is $\Delta_{0c}(p)$. Note how much less is the curvature in the latter case. Clearly the degree of curvature is a crucial factor in determining whether or not bows can exist from direct transmission. Rewriting Eq. (13) in terms of $r_i(p)$ for the profile Eq. (24), we have that

$$\Delta_{0l}(p) = 2p \int_{r_c(p)}^{1} \frac{\mathrm{d}r}{r(r^2n^2(r) - p^2)^{1/2}}. \tag{25}$$

For the $n(r)$ chosen here, $r_c(p)$ can be written explicitly as

$$r_i(p) = 2\left[1 - \left(1 - \frac{3p}{4}\right)^{1/2}\right]. \tag{26}$$

Such an explicit form can be readily found for any linear profile whether increasing or decreasing.

As seen in Figs. 2–4, specific radially dependent refractive index profiles may give rise to single or multiple extrema in the deviation functions $D_0(i)$ or $D_1(i)$. If one therefore wishes to determine what type of refractive index profile induces a particular "shape" for $D_0(p)$, e.g., a cubic function possessing at most two relative extrema, then $\Delta(p)$ is defined by Eq. (23), and from this, $n(r)$ can be found. It would be very convenient for theorists if the integral $I(\eta_i)$ [and hence $n(r)$] could be evaluated analytically every time, but this is not a major practical concern, since the integrals can be evaluated numerically. However, it should be noted that there are many such integrals tabulated for indefinite integrals corresponding to Eq. (22) with $\Delta(p)$ of the form p^m, where m is a positive or negative integer. Since $\arcsin p$ possesses a convergent power series expansion for $|p| \leq 1$, a series expansion for $\Delta(p)$ may be carried out as far as required, assuming $D_0(p)$ is also so expressed.

Although the focus of this paper has been the inversion of Θ, the interior ray deflection angle, to find the interior refractive index profile $n(r)$, this is easily related, via Eq. (23), to the more readily measured quantity D, the total deviation of the incident ray. This is possible because the surface boundary condition (via Snell's law of refraction) is incorporated implicitly in the equation for D. To see this, note that the expression (7) for $D_0(i)$ reduces to $D_0(i) = 2i - 2\tilde{r}(i)$, the standard result Eq. (9) when the refractive index is a constant inside the sphere. If the profile $n(r)$ is continuous within the particle—an assumption made throughout this paper—then the surface refractive index $n(1)$ is just the limit of the interior index as $r \to 1^-$, i.e., as r approaches 1 from within the sphere. Therefore, no additional information is in principle required to recover the complete profile. Note that, if the particle is a droplet of rapidly evaporating gasoline, then $n(1) = 1$ and $n'(1) = 0$, and the profile is continuous at the boundary, whereas if the particle is a water or ice sphere, then $n(1^-) > 1$ and $n(1^+) = 0$; i.e., the refractive index is discontinuous there.

5. Conclusion

It has been demonstrated that radially inhomogeneous spheres can, *in principle*, give rise to zero-order bows. Further work will be needed to determine how small the range of such variations needs to be in order for this to occur. It is certainly the case that the ranges of the refractive index profiles are somewhat arbitrary (between about 1.55 at or near the center and 1.1 at the surface). These profiles were chosen for illustrative purposes only and are not therefore representative of the kinds of particles that exist in nature. It is possible that particles composed of an ice/water combination will have approximate radial symmetry, but the refractive index will only vary between 1.31 and 1.33 (and it may not vary continuously). For typical sized droplets it seems unlikely that this would be sufficient to account for a zero-order bow. Nevertheless, it is hoped that future work will elucidate at least sufficient conditions for this to occur. Some progress has been made on this since [2], where it was pointed out that multiple primary bows can occur for a sufficiently negative value of $n'(r)$ inside the sphere. In this article it is shown that, for any specific deviation angle $D(i)$ (corresponding, say, to a single or multiple zero-order bow), the corresponding refractive index profile producing it in principle can be recovered. By extension, this also applies to higher-order bows.

Perhaps the most obvious potential applications of the results presented here are to rainbow refractometry and fiber optics. The latter was discussed quite extensively several decades ago (see [11–25] and in particular, [20,21,25]). For practical usage it would be of interest to add some random noise to $\Delta(p)$ representing uncertainties of measurement and see how this affects the recovered profile for $n(r)$. To some extent, and in a more general context, the numerical stability of Abel inversion has been discussed in [4,5,7,45] (extensions to discontinuous profiles have also been investigated [6,7]). This approach, perhaps coupled with the above-mentioned work could be usefully applied to current studies in fiber

optics and nanotechnology. Practical measurements of scattering will consist of a superposition of scattering modes such as direct reflection from the spherical surface, direct transmission, various rays that are reflected and refracted, as well as diffraction [13,17–19]. Any detailed analysis of the intensity of scattered light must include such contributions as well as incorporating the appropriately generalized Airy theory (for nonuniform spheres) or the use of the Lorenz–Mie theory, depending on whether a semiclassical or wave theoretic approach is taken [21,43,46]. In this ray-theoretic analysis, a complete separation of such modes was assumed in order to focus primarily on the mathematical technique. Three short appendices discuss details of the ray path integral and its connections with some other areas of mathematical physics.

Appendix A: Properties of $\eta(r)$ and Interpretation of the Ray Path Integral

A careful analysis of the integral (3) for $\Theta(i)$ in the neighborhood of the singularity yields two possibilities depending on whether or not $\eta(r)$ is a monotone increasing function.

i. Monotonic case. If $\eta'(r_c) \neq 0$, then, in the neighborhood of $r = r_c$, the integral for Θ has the dominant behavior $(r - r_c)^{1/2}$, which tends to zero as $r \to r_c^+$.

ii. Nonmonotonic case. If $\eta'(r_c) = 0$, then, in the neighborhood of $r = r_c$, the integral for Θ has the dominant behavior $\ln|r - r_c|$, which tends to $-\infty$ as $r \to r_c^+$.

To see this, we expand the quantity $r^2n^2(r)$ about the point $r = r_c$. The radicand then takes the form

$$r^2n^2(r) - K^2 = r_c^2n^2(r_c) - K^2 + \frac{d}{dr}[r^2n^2(r)]_{r_c}(r - r_c) + \frac{1}{2}\frac{d^2}{dr^2}[r^2n^2(r)]_{r_c}(r - r_c)^2 + O((r - r_c)^3). \quad \text{(A1)}$$

Simplifying (and neglecting extraneous multiplicative and additive constants) we find that, as indicated in Fig. 10, if $(d/dr[r^2n^2(r)])_{r_c} > 0$, then the integral in Eq. (3) has the functional form

$$I \propto \int (r - r_c)^{-1/2}dr \propto (r - r_c)^{1/2} \to 0, \quad \text{(A2)}$$

as $r \to r_c^+$. If, on the other hand, $(d/dr[r^2n^2(r)])_{r_c} = 0$, then

$$I \propto \int |r - r_c|^{-1}dr \propto \ln|r - r_c| \to -\infty, \quad \text{(A3)}$$

as $r \to r_c^+$.

Generic $\eta(r)$ profiles for these two cases are illustrated schematically in Figs. 10 and 11. In the monotonic case, the radius of closest approach for a given angle of incidence is denoted by r_i in Fig. 10; the distance of the ray trajectory from the center of the sphere is indicated on the r axis. This is also indicated in the nonmonotonic case in Fig. 11. To interpret Fig. 11, it is best to consider rays with angles of incidence increasing away from zero. The radius (point) of closest approach increases in a continuous manner until $i = i_2$, as shown. At that stage the point of closest approach increases discontinuously by an amount Δr to $r = r_c$, thereafter increasing continuously once again. This behavior corresponds to a spherical "zone" of thickness Δr into which *no rays* can penetrate. The situation is reversible: starting with $i = \pi/2$ and reducing, it yields the same zonal gap.

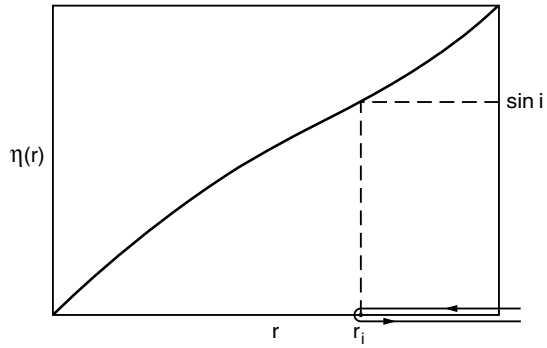

Fig. 10. $\eta(r) = rn(r)$ for the monotonic case. The point of closest approach is $r = r_c$.

In scattering theory, the logarithmic singularity (ii) is associated with the phenomenon of *orbiting*. An extremum of $\eta(r)$ arises at $r = r_c$ when

$$n'(r_c) = -\frac{n(r_c)}{r_c} < 0, \quad \text{(A4)}$$

meaning that the refractive index profile $n(r)$ either possesses a local minimum at $r = r_m > r_c$ or it tends monotonically to a constant value as r increases to 1 (see Fig. 12). Of course, unlike the case of classical and/or atomic or molecular scattering, $n(r)$ and its corresponding potential $V(r)$ is in general piecewise continuous. The orbiting behavior illustrated in Fig. 12 can be thought of as a type of "mechanical" version of a limit cycle in a dynamical system. The

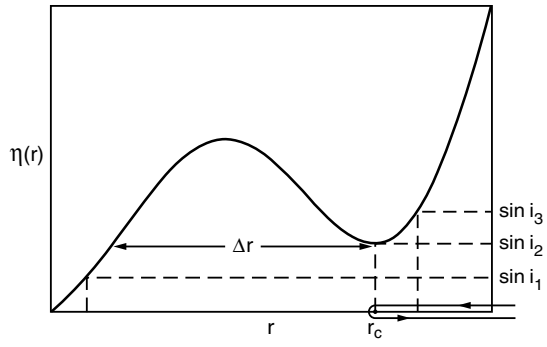

Fig. 11. $\eta(r) = rn(r)$ for the nonmonotonic case. The point of closest approach for $i > i_2$ is $r = r_c$, and a zone of width Δr exists into which no ray penetrates.

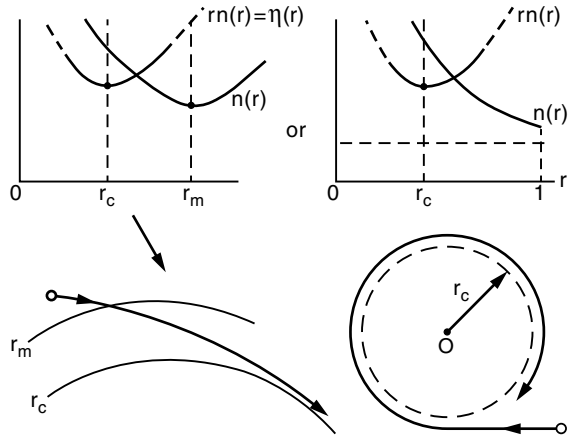

Fig. 12. Phenomenon of orbiting illustrated schematically associated with a zero of $\eta'(r)$.

connection between the two cases of "classical" and "potential" scattering is illustrated in Appendix B.

Appendix B: Connection with Classical Scattering and Gravitational Lensing

In the theory of classical scattering by a central force with potential $V(r)$, the total deflection angle θ is given by

$$\theta = \pi - 2b\int_a^\infty \frac{\mathrm{d}r}{r^2[1-b^2/r^2-V(r)/E]^{1/2}}, \tag{B1}$$

where b is the impact parameter, a is the distance of closest approach, and E is the particle energy. The integral can be recast to the optical case [see Eq. (3)] by setting $b = \sin i$ and

$$n(r) = \left[1-\frac{V(r)}{E}\right]^{1/2}, \tag{B2}$$

with $V(r) < 0$ corresponding to an attractive potential. Note that, since

$$n'(r) = \frac{-V'(r)}{2[1-V(r)/E]}, \tag{B3}$$

$V'(r) > 0$ corresponds to $n'(r) < 0$, the case of most interest here. This justifies the notion of a refracting sphere having the characteristics of a potential well, with implications for morphology-dependent resonances [48–50].

In the study of gravitational lenses, the field is said to be weak if the gravitational potential $V(\bar{r})$ satisfies the strong inequality $|V(\bar{r})|t \ll c^2$, c being the speed of light *in vacuo* [51]. In such a weak gravitational field, light is bent in accordance with an effective index of refraction given by

$$n(\bar{r}) = 1 - \frac{2V(\bar{r})}{c^2} + \ldots, \tag{B4}$$

where, for a spherically symmetric field, $V = -\mathrm{GM}/r$, so $n(r) \approx 1 + 2\mathrm{GM}/c^2 r$.

This time, formally substituting Eq. (B2) into Eq. (3), we obtain an approximate expression for the angular deflection of a ray due to the gravitational field, namely

$$\theta = \pi - 2\Theta \approx \pi - 2b\int_a^\infty \frac{\mathrm{d}r}{r^2[1+(2R_s/r)-(b^2/r^2)]}, \tag{B5}$$

where $R_s = 2\mathrm{GM}/c^2$ is the "gravitational radius." Clearly, in this weak field approximation the gravitational potential corresponds to an attractive $1/r$ potential. Therefore, the standard results from classical scattering apply;

$$\text{(i)}\quad \cot\left(\frac{\theta}{2}\right) = -\frac{b}{R_s}, \tag{B6}$$

and (ii), the geometrical optics "refraction cross section" is

$$\frac{d\sigma}{d\Omega} = \left|\frac{b\,db}{\sin\theta\, d\theta}\right| = \frac{R_s^2}{4\sin^4(\theta/2)}, \tag{B7}$$

where the impact parameter b greatly exceeds the gravitational radius. Note that, for small angles and impact parameters,

$$\theta = -\frac{2R_s}{b} = -\frac{4\mathrm{GM}}{c^2 b.}, \tag{B8}$$

a formula used to predict the deflection of light by the Sun [52].

Appendix C: Connection with Seismology and Refraction of Surface Gravity Water Waves

In seismological studies, the ray parameter p can be expressed in terms of T, the travel time of the ray. Δ and p are measured quantities, and $p = dT/d\Delta$. In this context, Eq. (13) is a convenient form for numerical integration using a tabulation of travel times in equal intervals of Δ. Equation (17) determines r_i corresponding to Δ_i, and hence $\eta_i = r_i/v_i$, where $v(r)$ is the velocity profile for this class of waves. Hence, $v(r)$ can be determined down to the level of maximum ray penetration of the seismic ray [38–40].

Since $T = \int \mathrm{d}s/v$ taken along the ray, it is readily established that

$$T = 2\int_{r_i}^{r_0} \frac{\eta^2}{r(\eta^2-p^2)^{1/2}}\,\mathrm{d}r$$

$$= 2\int_{r_i}^{r_0} \{p^2 r^{-1}(\eta^2-p^2)^{-1/2} + r^{-1}(\eta^2-p^2)^{1/2}\}\mathrm{d}r, \tag{C1}$$

$$= p\Delta + 2\int_{r_i}^{r_0} r^{-1}(\eta^2-p^2)^{1/2}\mathrm{d}r. \tag{C2}$$

A constraint must be imposed on $v(r)$ such that the travel time curve $(T - \Delta)$ is everywhere continuous and single valued. In seismological terms this constraint is $0 < dv/dr < v/r$. Since $v(r) \propto n(r)^{-1}$, it is easily seen that this constraint is equivalent to the condition $(rn(r))' > 0$, i.e., $\eta'(r) > 0$, which is just the requirement for monotonicity and uniqueness discussed in Section 3. Violations of this condition occur at the core–mantle boundary (at a depth of about 2900 km [39]), and this can cause a ray gap or shadow zone and consequently a break in the travel time curve.

An equation identical to Eq. (3) arises in the theory of refraction of surface gravity water waves by islands and submerged reefs or shoals with circular symmetry [53]. Not surprisingly, the rays, orthogonal to the wavefronts, are refracted by the varying underwater topography in an exactly analogous manner to the optical rays discussed here. The analog of the refractive index $n(r)$ is the local wavenumber $k(r)$ associated with the variable depth $h(r)$. The dispersion relation for such waves is [53,54]

$$\omega = (gk \tanh kh)^{1/2}, \tag{C3}$$

g being the gravitational acceleration and ω being the (constant) angular frequency of the wave. In very shallow water, $k \propto h^{-1/2}$, and provided that $rh^{-1/2} \to 0$ as $r \to 0$, then kr also $\to 0$ as $r \to 0$ (note that here $kr = \eta$). Since $k'(r) < 0$ here, the ray paths will be qualitatively similar to those in Fig. 6. A submerged circular shoal falls into this category [53]. In the case of a circular island, for which at some radius b, say, $h(b) = 0, k \to \infty$ as $r \to b^+$. If however the depth has a constant value for some $r > b$, then k has a constant value and $kr \propto r$. Therefore, the $\eta(r)$ graph has a minimum (and possibly more), and, as discussed in connection with a "ray-free" zone in Appendix A, rays sufficiently close to the island will reach the shore, while those further away will be "repelled" by the island without reaching the shore. Furthermore, if the $\eta(r)$ graph is qualitatively similar to that shown in Fig. 11, waves generated within an annular region Δr will become trapped in that region. There is no equivalent situation in the optical problem discussed here since the rays are externally incident upon the sphere, but if the undersea floor has the shape of a ring-shaped ridge, this surface wave phenomenon can certainly occur.

References

1. J. A. Lock and T. A. McCollum, "Further thoughts on Newton's zero-order rainbow," Am. J. Phys. **62**, 1082–1089 (1994).
2. J. A. Adam and P. Laven, "Rainbows from inhomogeneous transparent spheres: a ray-theoretic approach," Appl. Opt. **46**, 922–929 (2007).
3. M. Deutsch and I. Beniaminy, "Derivative-free inversion of Abel's integral equation," Appl. Phys. Lett. **41**, 27–28 (1982).
4. M. Deutsch and I. Beniaminy, "Inversion of Abel's integral equation for experimental data," J. Appl. Phys. **54**, 137–143 (1983).
5. M. Deutsch, "Abel inversion with a simple analytic representation for experimental data," Appl. Phys. Lett. **42**, 237–239 (1983).
6. M. Deutsch, A. Notea, and D. Pal, "Reconstruction of discontinuous density profiles of cylindrically symmetric objects from single x-ray projections," Appl. Opt. **27**, 3962–3964 (1988).
7. M. Deutsch, A. Notea, and D. Pal, "Abel reconstruction of piecewise constant radial density profiles from x-ray radiographs," Appl. Opt. **28**, 3183–3186 (1989).
8. M. Deutsch, A. Notea, and D. Pal, "Inversion of Abel's integral equation and its application to NDT by x-ray radiography," NDT Int. **23**, 32–38 (1990).
9. M. A. Sharaf, A. A. Sharaf, and H. Selim, "Analytical solution of Abel's equation for stellar density in globular clusters," Rom. Astr. J. **14**, 107–114 (2004).
10. V. R. Eshleman, E. M. Gurrola, and G. F. Lindal, "On the black hole lens and its foci," Adv. Space Res. **9**, 119–122 (1989).
11. M. Kerker and E. Matijevic, "Scattering of electromagnetic waves from concentric infinite cylinders," J. Opt. Soc. Am. **51**, 506–508 (1961).
12. J. L. Lundberg, "Light scattering from large fibers at normal incidence," J. Colloid Interface Sci. **29**, 565–583 (1969).
13. H. M. Presby, "Refractive index and diameter measurements of unclad optical fibers," J. Opt. Soc. Am. **64**, 280–284 (1974).
14. L. S. Watkins, "Scattering from side-illuminated clad glass fibers for determination of fiber parameters," J. Opt. Soc. Am. **64**, 767–772 (1974).
15. D. Marcuse and H. M. Presby, "Light scattering from optical fibers with arbitrary refractive-index distributions," J. Opt. Soc. Am. **65**, 367–375 (1975).
16. J. W. Y. Lit, "Radius of uncladded optical fiber from backscattered radiation pattern," J. Opt. Soc. Am. **65**, 1311–1315 (1975).
17. D. Marcuse, "Light scattering from unclad fibers: ray theory," Appl. Opt. **14**, 1528–1532 (1975).
18. P. L. Chu, "Determination of the diameter of unclad optical fibre," Electron. Lett. **12**, 14–16 (1976).
19. P. L. Chu, "Determination of diameters and refractive indices of step-index optical fibres," Electron. Lett. **12**, 155–157 (1976).
20. P. L. Chu, "Nondestructive measurement of index profile of an optical-fibre preform," Electron. Lett. **13**, 736–738 (1977).
21. C. Saekeang and P. L. Chu, "Backscattering of light from optical fibers with arbitrary refractive index distributions: uniform approximation approach," J. Opt. Soc. Am. **68**, 1298–1305 (1978).
22. D. Marcuse, "Refractive index determination by the focusing method," Appl. Opt. **18**, 9–13 (1979).
23. D. Marcuse and H. M. Presby, "Focusing method for nondestructive measurement of optical fiber index profiles," Appl. Opt. **18**, 14–22 (1979).
24. H. M. Presby and D. Marcuse, "Optical fiber preform Diagnostics," Appl. Opt. **18**, 23–30 (1979).
25. C. Saekeang and P. L. Chu, "Nondestructive determination of refractive index profile of an optical fiber: backward light scattering method," Appl. Opt. **18**, 1110–1116 (1979).
26. R. A. Phinney and D. L. Anderson, "On the radio occultation method for studying planetary atmospheres," J. Geophys. Res. **73**, 1819–1827 (1968).
27. G. Fjeldbo, A. J. Kliore, and V. R. Eshleman, "The neutral atmosphere of Venus as studied with the Mariner V radio occultation experiments," Astron. J. **76**, 123–140 (1971).

28. V. R. Eshleman, "The radio occultation method for the study of planetary atmospheres," Planet. Space Sci. **21**, 1521–1531 (1973).
29. S. B. Healy, J. Haase, and O. Lesne, "Abel transform inversion of radio occultation measurements made with a receiver inside the Earth's atmosphere," Ann. Geophys. **20**, 1253–1256 (2002).
30. G. A. Hajj, E. R. Kursinski, L. J. Romans, W. I. Bertiger, and S. S. Leroy, "A technical description of atmospheric sounding by GPS occultation," J. Atmos. Sol. Terr. Phys. **64**, 451–469 (2002).
31. P. Guo, H-J. Yan, Z-J. Hong, M. Liu and C. Huang, "On the singular points of the Abelian integral transformation in the GPS/LEO occultation technique," Chinese Astron. Astrophys. **28**, 441–448 (2004).
32. F. Xie, J. S. Haase, and S. Syndergaard, "Profiling the atmosphere using the airborne GPS radio occultation technique: a sensitivity study," IEEE Trans. Geosci. Remote Sens. **46**, 3424–3435 (2008).
33. S. C. Solomon, P. B. Hays, and V. J. Abreu, "Tomographic inversion of satellite photometry," Appl. Opt. **23**, 3409–3414 (1984).
34. K. Bockasten, "Transformation of observed radiances into radial distribution of the emission of a plasma," J. Opt. Soc. Am. **51**, 943–947 (1961).
35. W. L. Barr, "Method for computing the radial distribution of emitters in a cylindrical source," J. Opt. Soc. Am. **52**, 885–888 (1962).
36. P. W. Schreiber, A. M. Hunter, and D. R. Smith, Jr., "The determination of plasma electron density from refraction measurements," Plasma Phys. **15**, 635–646 (1973).
37. C. J. Tallents, M. D. J. Burgess, and B. Luther-Davies, "The determination of electron density profiles from refraction measurements obtained using holographic interferometry," Opt. Commun. **44**, 384–387 (1983).
38. K. E. Bullen, *Introduction to the Theory of Seismology*, 3rd ed. (Cambridge University, 1965).
39. F. D. Stacey, *Physics of the Earth*, 2nd ed. (Wiley, 1977).
40. C. B. Officer, *Introduction to Theoretical Geophysics* (Springer-Verlag, 1974).
41. C. L. Brockman and N. G. Alexopoulos, "Geometrical optics of inhomogeneous particles: glory ray and the rainbow revisited," Appl. Opt. **16**, 166–174 (1977).
42. M. Marklund, D. Anderson, F. Cattani, M. Lisak, and L. Lundgren, "Fermat's principle and the variational analysis of an optical model for light propagation exhibiting a critical radius," Am. J. Phys. **70**, 680–683 (2002).
43. M. R. Vetrano, J. P. van Beeck, and M. Riethmuller, "Generalization of the rainbow Airy theory to nonuniform spheres," Opt. Lett. **30**, 658–660 (2005).
44. C. M. Vest, "Tomography for properties of materials that bend rays: a tutorial," Appl. Opt. **24**, 4089–4094 (1985).
45. W. Glantschnig, "How accurately can one reconstruct an index profile from transverse measurement data?" J. Lightwave Technol. **3**, 678–683 (1985).
46. M. R. Vetrano, J. P. van Beeck, and M. L. Riethmuller, "Assessment of refractive index gradients by standard rainbow thermometry," Appl. Opt. **44**, 7275–7281 (2005).
47. X. Li, X. Han, R. Li, and H. Jiang, "Geometrical-optics approximation of forward scattering by gradient-index spheres," Appl. Opt. **46**, 5241–5247 (2007).
48. R. G. Newton, *Scattering Theory of Waves and Particles* (Springer-Verlag, 1982).
49. H. M. Nussenzveig, *Diffraction Effects in Semiclassical Scattering* (Cambridge University, 1992).
50. W. T. Grandy, Jr., *Scattering of Waves from Large Spheres* (Cambridge University, 2000).
51. D. Drosdoff and A. Widom, "Snell's law from an elementary particle viewpoint," Am. J. Phys. **73**, 973–975 (2005).
52. M. Berry, *Principles of Cosmology and Gravitation* (Cambridge University, 1976).
53. C. C. Mei, *The Applied Dynamics of Ocean Surface Waves* (World Scientific, 1989).
54. J. A. Adam, *Mathematics in Nature: Modeling Patterns in the Natural World* (Princeton University, 2006).